


<https://doi.org/10.1038/s43247-024-01290-1>

Anti-repeating earthquakes and how to explain them

Simone Cesca¹ , Peter Niemz^{1,2}, Torsten Dahm^{1,3} & Satoshi Ide⁴

Repeating earthquakes, or repeaters, affecting overlapping rupture patches with a similar focal mechanism, have important implications to track fault slip rates, aseismic deformation, slow earthquakes and earthquake nucleation processes. They are often detected based on highly similar waveforms. Here, we discuss earthquakes with highly anti-correlated waveforms, denoting a reversed seismogenic process at the same or a neighbouring location, which we refer to as true and quasi anti-repeaters. We first report a range such observations in different environments, including volcano seismicity, intermediate depth seismicity and injection-induced microseismicity. Then, we review conceptual models proposed to explain them. True and quasi anti-repeaters can be robustly identified via a three-component single station or distributed network data. They are key indicators for stress perturbation transients or local stress heterogeneities. Since most of these observations were explained as the response to fluid migration processes, they may help to identify and track fluid movements in the subsurface.

Repeating earthquakes, or repeaters, are defined as earthquakes with overlapping rupture areas, sharing a similar location, magnitude and focal mechanism^{1–3}. Due to the similarity of their sources, they generally produce highly similar waveforms^{1–7}. Indeed, while a robust identification of true repeaters may require accurate hypocentral locations and focal mechanism estimations^{2,3}, it has been a common practice in the past to detect and identify repeaters simply based on a high cross-correlation of their waveforms. A robust approach to discriminate among true repeaters and neighbouring events (quasi-repeaters) with a similar focal mechanism has been recently designed³. Repeaters have been observed in different tectonic environments^{4,6–10} and most notably at different subduction zones, where they are attributed to the repeated activation of asperities along the slab interface^{11,12}. Their analysis and modelling have turned out to be very important in revealing, mapping and quantifying fault slip^{13,14} and as possible earthquake precursors^{15,16}. Seismic events with similar waveforms are sometimes also referred to as multiplets^{17–21}. While repeaters are assumed to have overlapping rupture areas and a similar slip, waveform similarity criteria to robustly identify them are still debated^{1–3,22}.

Here, we investigate the case of earthquake pairs (or earthquake families) displaying anti-correlated waveforms. Consistently with the case of earthquake repeaters, we define anti-repeaters as earthquakes which can be robustly attributed to the reverse slip of the same patch or fault segment, with a difference in location much smaller than the source size, and opposite focal mechanisms. We also consider the case of quasi anti-repeaters, which

represent a failure with a reversed focal mechanism occurring within a small seismogenic volume, but affecting neighbouring faults or fault portions.

Both cases, true and quasi anti-repeaters, are manifested in highly anti-correlated seismic waveforms. The literature on such phenomena is still limited. The term ‘anti-repeater’ has been first used, to our knowledge, for describing such observations at the Bucaramanga nest, Colombia^{23,24}, where their presence was confirmed by similar waveforms with reversed polarities at multiple stations²⁴. A few more observations are discussed for seismicity associated with magmatism. For example, during the January 1983 magmatic intrusion at Kilauea, Hawaii, a number of earthquake multiplets were detected, including one with two groups of earthquakes with correlated and anti-correlated waveforms, associated with events with nearly opposite focal mechanisms¹⁹. Earthquakes with reversed waveforms were reported during deep crustal seismic sequences²⁵ and swarms²⁶, which were attributed to magma intrusion of fluid pressure pulses^{25,26}. More recently, anti-correlated waveforms have been reported²⁷ during the seismic swarm accompanying a magmatic intrusion offshore Mayotte, Comoro Islands^{27–29}. Relatively sparse accounts for anti-repeaters might be caused by the fact that most studies applying waveform cross-correlation only use the maximum cross-correlation or reject the polarity³⁰. When using cross-correlation to improve relative timing information for subsequent relative earthquake location, the rejection can make sense. However, it leads to a loss of relative information regarding the faulting mechanism. Only a few studies^{26,31} take into account the minimum correlation that can reveal anti-correlated events. With our

¹GFZ German Research Centre for Geosciences Potsdam, Potsdam, Germany. ²University of Utah, Salt Lake City, UT, USA. ³University of Potsdam, Potsdam, Germany. ⁴University of Tokyo, Tokyo, Japan. ✉e-mail: simone.cesca@gfz-potsdam.de

study, we intend to increase the awareness for the importance of both the positive and the negative part of the widely used cross-correlation function to study earthquake processes.

In the lack of a dedicated local network, a physics based identification of repeaters, relying on accurate locations and rupture size estimation^{2,3} is challenging. On the other hand, identifying repeaters from waveforms only requires accomplishing certain cross-correlation coefficients and the processing of high frequency signals²², which constrain this type of observation to relatively small earthquakes only. While the same arguments would also apply to anti-repeaters, in this work we chose to relax the conditions on the frequency content of the seismic records, adapting them to each considered observational setup. We choose the bandpass filters with the primary aim of preserving a good signal-to-noise ratio, and ensuring that the high frequency corner is below the earthquake corner frequencies. Adopting these smoother conditions implies that not all discussed cases may be strictly considered anti-repeaters, but some may correspond to quasi anti-repeaters and, in other cases, a discrimination is not possible based on the available data. We will discuss, however, how both anti-repeaters and quasi anti-repeaters require strong spatial and/or temporal stress perturbations, so that searching for both types of process is relevant.

If the literature on direct observation of earthquakes with anti-correlated waveforms is limited, there are a few more reports on earthquakes with reversed or rotated focal mechanisms within the same seismogenic volume^{32–43}. Again, many of these observations concern volcano seismicity, triggered by dike intrusions at different depths, ranging from deep crustal intrusion to shallow processes. Almost reversed, composite focal mechanisms have also been identified for microseismicity accompanying hydraulic fracturing⁴⁴. Reversed mechanisms at similar locations generally imply anticorrelated waveforms. Reversed mechanisms are not limited to double-couple focal mechanisms, but have also been observed for moment tensor representations. Reversed moment tensors resolved for different onsets during the 2022 Hunga Tonga eruption⁴³ could correspond to explosions and caldera collapse episodes. Reversed vertical symmetric CLVD sources at

Bardarbunga volcano, Iceland, have been interpreted as the reversed motion of a ring fault, accompanying e.g., inflation and deflation phases of the volcanic system^{45,46}. In the frame of tectonic processes, focal mechanism reversals have been reported more sporadically and generally attributed to stress changes induced by large earthquakes and overshooting^{47,48}. Studies on hydraulic fracturing^{49,50} and enhanced geothermal systems^{20,51} commonly observe multiplets or repeating events, but anti-correlated events are only considered in a few studies^{52–54}. Finally, it is worth noting that events with polarity reversal within the same cluster were reported for deep moonquakes⁵⁵.

Starting from a collection of earthquakes with anti-correlated waveforms in different seismogenic contexts, spanning a wide variety of frequencies, magnitudes and observational setups, we review different models proposed to explain the observation of earthquakes with reversed slip motion. We discuss some challenges to identify anti-repeaters (as well as repeaters) based on waveform anti-correlation. Finally, we discuss the important implications of anti-repeaters.

Observations

The following cases concern volcanic, tectonic, intermediate depth and induced seismicity cases (Tables 1 and 2).

North Mid-Atlantic Ridge

The 2022 swarm at the north Mid-Atlantic Ridge has been described as the result of a shallow magmatic intrusion⁵⁶, with the consequent activation of normal faulting earthquakes above a vertical dike and a few thrust earthquakes triggered by stress perturbation at the side of the growing dike, with a lateral offset of ~10–20 km. Earthquakes exceeding magnitude Mw 4.5 were classified based on their moment tensors, with 60 events characterised by North-South (NS) oriented normal faulting, and 11 events by NS thrust mechanisms⁵⁶. The seismic signals, recorded at up to 2500 km distance, with the closest station at ~1000 km, were found to be anti-correlated between the two families⁵⁶. This is consistent with the flipped focal mechanism, the

Table 1 | Anti-repeaters parameters

Case	Difference		Range of distances	Bandpass Filter [Hz]	Dominant frequency [Hz]*	Shear wave velocity in source volume [m/s]	$\lambda/4$ [m]	Anti-CC/CC (mean of 3 components/stations)
	Time	Space [m]						
Mid Atlantic Ridge	~4.5 d	45500	1106–1123 km	0.02–0.1	~0.05	3900	78000	–0.89/0.59
Bucaramanga	~3.5 d	11500	~186 km	0.375–4.0	~0.5	4500 (*mantle)	9000	–0.99/0.67
Mayotte	84 s	~ 600	~30 km	0.4–4.0	~2.5	4000 (*lower crust)	1600	–0.92/0.70
Äspö HRL	6 s	0.45	10.8–16.6 m	3000–7000	~ 5000	3200	0.64	–0.93/0.85

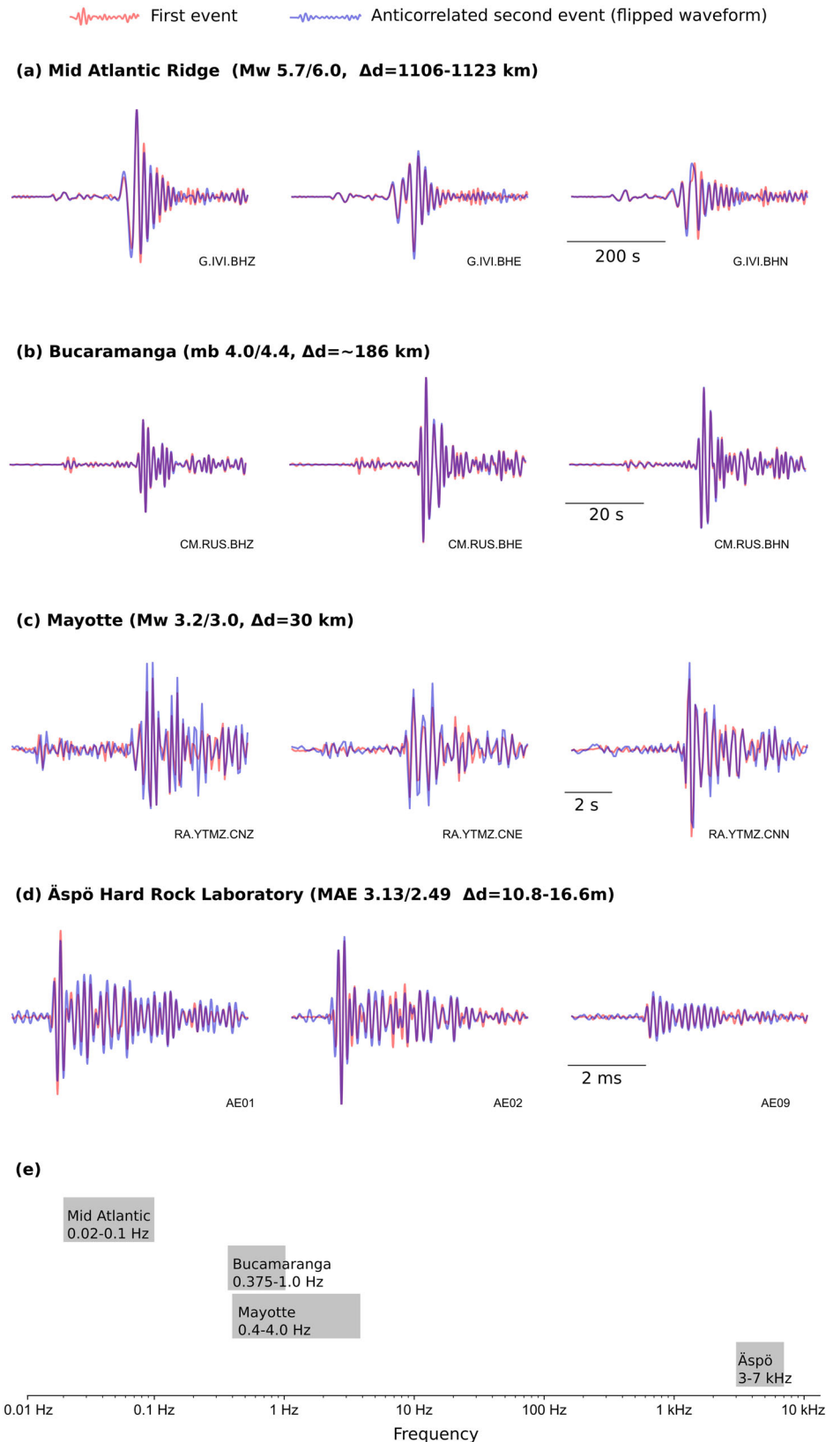
The table reports for each earthquake pairs the following information: region, hypocentral offset, inter-event time, range of distances to the stations recording anti-correlated data (epicentral distances for the Mid Atlantic Ridge, hypocentral distances for the other case studies), bandpass filter, dominant frequency, S wave velocity in the focal region, quarter wavelength, CC_{min} and CC_{max}.

Table 2 | Earthquake parameters

Date	Time	Region	Lat	Lon	Depth [km]	Magnitude	Reference
2022-09-26	09:59:57	Mid Atlantic Ridge	54.0141	–35.3224	6.3	Mw 5.7	Cesca et al. 2023
2022-10-01	01:18:55	Mid Atlantic Ridge	53.6602	–35.6690	4.9	Mw 6.0	
2018-08-31	18:21:55	Bucaramanga	6.8262	–73.1078	154.5	mb 4.0	ISC-REV
2020-09-04	04:58:19	Bucaramanga	6.7707	–73.0260	158.0	mb 4.4	NEIC
2018-08-20	21:34:15	Mayotte	~12.80	~45.43	~20	Mw 3.2	Cesca et al. 2022
2018-08-20	21:35:39	Mayotte	~12.80	~45.43	~20	Mw 3.0	
			X [m]	Y [m]	Z [m]		
2015-06-04	08:50:33.402	Äspö HRL	2402.7	7307.4	405.9	M _{AE} 3.13	Niemz et al. 2020
2015-06-04	08:50:39.482	Äspö HRL	2403.2	7307.2	405.9	M _{AE} 2.49	

The table reports for each earthquake the following information: date, time, region, hypocentral coordinates, magnitude and reference for the location and magnitude.

Fig. 1 | Examples of anti-repeaters. Four cases are reported: **a**, Mid Atlantic Ridge, **b**, Bucaramanga, Colombia, **c**, Mayotte, Comoro Islands, and **d**, Äspö Laboratory, Sweden. For each observation we show three sets of traces, for different components or stations, as reported in the bottom right of each plot. Raw waveforms (velocity in **a** and **b**, acceleration in **c**, counts in **d**) are plotted, after applying a bandpass filter (as reported in **e**). In each panel, two waveforms are plotted: the first event in red and the second one in blue, after waveform flipping. Waveforms are normalised preserving the amplitude ratios among different traces at the same site.



small inter-event distance compared to the source-receiver distances and the good signal-to-noise ratio limited to low frequencies. We show here an example of three component anti-correlated waveforms at the broadband seismic station G.IVI.00 (GEOSCOPE, French Global Network of

Seismological Broadband Stations⁵⁷), located at ~1100 km distance, filtered in the frequency range 0.02-0.1 Hz. The normalised velocity data are compared for two earthquakes of moment magnitude Mw 5.7 and 6.0⁵⁶ (Fig. 1a and Suppl. Figures 1-2).

Bucaramanga, Colombia

Earthquake nests are volumes of the Earth characterised by high, persistent and spatially isolated seismic activity⁵⁸. The Bucaramanga nest, Colombia, is the most dense seismic nest on Earth⁵⁹. There, an average of 8 events per year (with body wave magnitudes larger than mb 4.7)⁶⁰ within a compact volume extending only 5 × 5 km laterally and less than 20 km in depth^{24,59}. Based on a selection of well-located earthquakes, the focal region has been hypothesised to be even smaller⁶¹, 4 × 4 × 8 km. Focal mechanisms at the Bucaramanga nest are reported to be heterogeneous²⁴. Thanks to its compact size, which grants similar hypocentral locations, and the variability of focal mechanisms, the Bucaramanga nest is a good place to search for anti-repeaters. The presence of families of both earthquakes with correlating and anti-correlating waveforms at the Bucaramanga nest was indeed found in a previous study²⁴, where the high anti-correlation was simultaneously confirmed on five stations. Earthquake locations would suggest they activated parallel, neighbouring ruptures. However, the inter-event distances, in the order of ~1–2 km are comparable to relocation uncertainties, so it was not possible to discriminate among true and quasi anti-repeaters²⁴. Here, we perform a similar search for anti-correlated waveforms and illustrate one case of three components anti-correlated waveforms for a pair of events (Fig. 1b, Suppl. Figure 3–4). The two selected earthquakes had moderate magnitudes (mb 4.0 and 4.4) and depths of 155 and 158 km. Waveforms are shown after applying a bandpass filter between 0.375 and 1.0 Hz.

Mayotte, Comoro Islands

The recent volcano-tectonic unrest offshore the island of Mayotte^{27,28}, Comoros Islands, is most notably known for the global observation of long-duration long period signals^{27,28} and for the formation and discovery of a newborn submarine volcano²⁹. However, there was evidence for multiple earthquake pairs with anti-correlated waveforms among the different seismic signals recorded during the unrest²⁷. Here, we show one example of an event pair with anti-correlated waveforms at Mayotte (Table 1). The seismic signals show volcano-tectonic signatures, with clear P and S onsets (Fig. 1c, Suppl. Figs. 5–6); they were recorded at the YTMZ strong motion sensor, on Mayotte island, with a waveform duration of ~8–10 s and a good signal-to-noise ratio in the range 0.4–4.0 Hz. The location of these earthquakes is unknown, because they were recorded by this station only and data quality prevented an accurate single station location. Based on the differential S-P times at station YTMZ (3.67 and 3.75 s), we infer a minimum distance of ~600 m between the hypocenters of the event pair. This distance is larger than the rupture length of these events, estimated as ~300–400 m from their magnitudes (~3.2 and ~3.0), based on empirical relations⁶². Their focal mechanisms have not been estimated⁶³. The earthquake pair (Fig. 1c) occurred after the crustal intrusion reached the seafloor, in the early phase of the deep reservoir drainage²⁷. The earthquake pair pertain to the so-called proximal cluster, located between 6 and 20 km East of Petite-Terre (Mayotte), and mostly extending at 25–45 km depth⁶⁴; however, the seismic activity was found between 4 and 24 km at the end of August⁶⁴, when the earthquake pair occur. It has been hypothesised that these earthquake pair occurred just above the depleting reservoir, in response to changes in the reservoir's pressure²⁷. They occurred within a short time, in the order of one minute: short inter-event times for event pairs with reversed waveforms were also found during deep crustal seismic swarms driven by magma intrusions beneath Mammoth Mountain, California²⁶.

Åspö Hard Rock Laboratory, Sweden

Observations of anti-repeating earthquakes are not limited to local or regional seismicity. We also identified such event pairs within massive acoustic emission (AE) activity (tiny earthquakes, here below Mw –3.5) induced during small-scale hydraulic fracturing experiments conducted in crystalline rock⁶⁵. There, more than 19,600 induced events mapped the opening hydraulic fractures with extents of several metres^{66,67}. While an inversion for focal mechanisms is difficult to assess due to uncertainties in sensor characteristics⁶⁸, waveform similarity analysis conducted in this study reveal the presence of anti-correlated events/anti-repeaters within the

spatially and temporally constrained event cluster. The two example events (Fig. 1d) were induced within 6 seconds during an injection phase, in which the hydraulic fracture grew upwards and eventually passed the location of the two events. The absolute event locations indicate a separation of 0.45 m, which is well within the location uncertainty of the catalogue⁶⁶. The anti-repeaters have anti-correlated waveforms within a frequency band of 3 to 7 kHz across three sensors at distances of 10 to 16 m. The two events have relative AE magnitudes of M_{AE} 3.13 and M_{AE} 2.49, which corresponds⁶⁹ to about Mw –4. Example waveforms are presented in Fig. 1d and Suppl. Figs. 7–8. Instances of reversed focal mechanisms in close vicinity to each other were also reported for microseismic activity induced during shale gas hydraulic fracturing⁵³.

Models

Several physical processes have been considered to explain strong local stress anomalies and the occurrence of earthquakes with reversed or rotated focal mechanisms. Stress anomalies can be temporal or spatial, but a temporal stress perturbation is needed if the rupture occurs over the same patch (e.g., in the case of true anti-repeaters). Most of these models concern volcanic and induced seismicity, driven by geophysical processes involving deformation, magma migration and/or fluid transfer. Some, however, involve the effects produced by large earthquakes, and may become relevant in other tectonic settings. For each of the aforementioned processes, the occurrence of anti-repeaters depends on the local stress conditions and in some cases the presence of preexisting sets of faults, fractures or otherwise weakened zones with a particular orientation. In the following, we review those underlying physical processes and the most prominent models (Fig. 2) proposed in the literature. In some models, anti-repeaters are controlled by stress rotation due to dike emplacement and growth (Fig. 2a, b). In other cases anti-repeaters correspond to reverse motion along pre-existing zones of weakness (Fig. 2c, g).

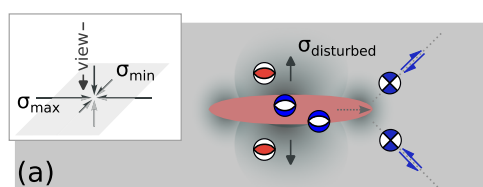
Dike intrusion and growth

Magmatic intrusions can produce strong local stress perturbations and induce seismicity, which vary with time, as the intrusion propagates, thickens, deforms, bends and/or freezes^{70–73}. The stress induced by such intrusions (dikes or sills) is spatially heterogeneous. For example, a vertical dike promotes extensional stresses above and below it, favouring normal faulting earthquakes. A lateral migrating vertical dike favours strike-slip earthquakes ahead of its tip⁷⁴, but these weakened regions can experience a different stress condition when the dike propagates. A thickening dike can alter compressional stresses on its sides⁷⁴: small dike inflation in the order of 1 m may be sufficient to produce a ~90° stress rotation and thus rotated focal mechanisms, as observed at several volcanoes^{33,42,76–79}; such stress perturbation is further promoted in the presence of highly viscous magmas⁴¹. The close location of rotated and unrotated focal mechanisms suggests a locally heterogeneous stress field, possibly involving a crack network, rather than a single conduit or crack³³. Something similar happens in the case of fluid injection operations, e.g., accompanying hydraulic fracturing or geothermal stimulation, which is discussed later. In both volcanic and injection induced seismicity cases the stress field is both controlled by background tectonic stresses and the stress perturbations introduced by the emplacement and migration of the dike or pressurised fluid. However, in the case of magma dikes, with average thickness in the order of tens of centimetres or more, locally reaching kilometres of lateral extension⁷⁵, the stress perturbation may overcome the tectonic stresses⁵⁶; while for fluid injection operations the stress perturbation is limited to a small volume around the injection point.

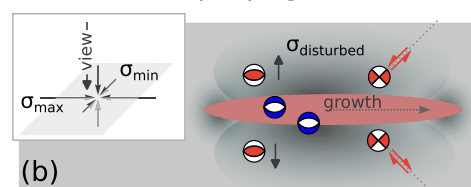
Figure 2a, b provides a sketch of a dike intrusion and migration, highlighting the regions of stress perturbation and the focal mechanisms of induced seismicity promoted around the dike. Shallow normal faulting earthquakes often accompany dike migration and are generally observed above vertical dikes⁷⁴. On the sides of the dike the stress perturbation inhibits normal faulting earthquakes, and can sporadically favour thrust faulting⁵⁶, providing a first model for quasi anti-repeaters, here occurring on different,

Local stress rotation

Dike intrusion

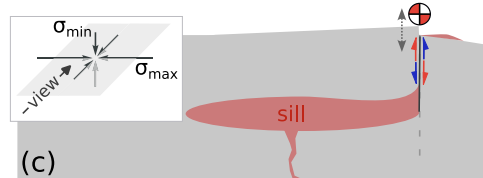


Further dike propagation

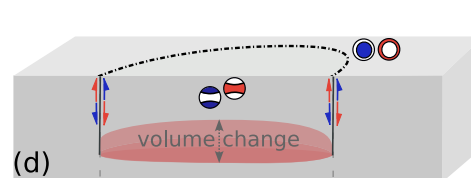


Opposite slip at pre-existing zones of weakness

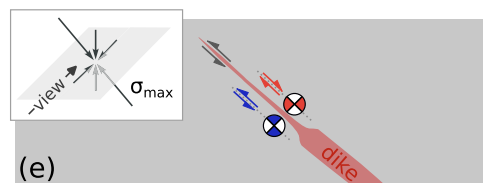
Trapdoor faulting



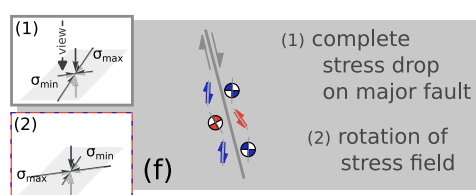
Ring faulting



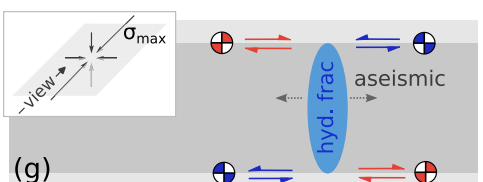
Dike parallel joints



Complete stress drop



Bedding planes



Steep graben-like structures

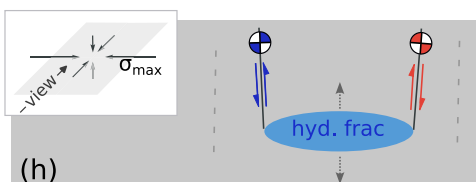


Fig. 2 | Proposed conceptual models for anti-repeating events. **a** and **b**, Local stress rotation upon dike intrusion and growth^{33,73}, **c**, Trapdoor faulting⁸¹, **d**, Ring faulting⁴⁶, **e**, Dike parallel joints³⁸, **f**, Stress rotation after complete stress drop⁴⁷, **g**, Bedding plane slip^{53,54}, **h**, Steeply dipping shear fractures³⁴.

parallel faults. Also true anti-repeaters can occur as a consequence of spatio-temporal stress perturbations, upon the migration of a magma batch: in these cases, strike-slip earthquakes can first be triggered along a zone of weakness ahead of the dike's tip (Fig. 2a, blue strike-slip mechanism) and then with reverse motions of the same structure when the dike grows or propagates forward (Fig. 2b, red strike-slip mechanism).

Trapdoor faults

Trapdoor faulting (Fig. 2c) represents a suitable model to explain true anti-repeaters. Trapdoor faults have been proposed for volcanic environments, requiring a combination of vertical deformation, e.g., uplift or subsidence due to the expansion or depletion of a magma body, and shallow faulting^{80–84}. The trapdoor faulting process (Fig. 2c) has been modelled for intruding sills, with a lateral extension equal or larger than their depths. In such cases, the magmatic intrusion can bend and propagate upward, favouring faulting on outward-dipping or sub-vertical normal faults due to the intrusion interaction with the free surface⁸¹. A focal mechanism reversal on a trapdoor fault could occur, e.g., in response to a later depletion of the magma body. A well-described case of trapdoor

faulting is found at Sierra Negra volcano, Galápagos, affecting intracaldera fault in response to a rapid caldera uplift⁸². While at Sierra Negra, there was so far no evidence of a reversed motion of the fault, which was so far accompanied by uplift only and behaved predominantly aseismically⁸⁰, monitoring the behaviour of trapdoor faults could offer other observations of anti-repeating earthquakes. Alternating slip along a trapdoor fault, accompanying the progressive failure of the overburden above a large and relatively deep depleting magma reservoir, has been hypothesised to explain the anti-correlated seismic signals at Mayotte²⁷ (Fig. 1c). There, the short interevent time among earthquakes producing reversed signals would rather point to an intermittent pressurisation of the reservoir, with upward movement accompanying pressurisation and downward movement following pressure drop, e.g., due to gas release. The focal mechanism of a trapdoor faulting earthquake is close to a vertical dip slip mechanism (Fig. 2c), which can turn into a steep normal or thrust faulting, depending on the fault geometry and whether the deformation involves an uplift or subsidence. Here potential anti-repeaters may be observed at different times, as reversed slip of the fault can be promoted during different deformation stages.

Ring faults

A trapdoor fault extending along a curved fault segment or even a circular or elliptical fault (Fig. 2d) is often referred to as a ring fault segment or ring fault^{46,85}. Ring faults are typically formed on top of magmatic reservoirs and can accompany the formation of calderas. A slip along the whole ring fault is described by a vertical compensated linear vector dipole (vCLVD)^{46,85}. Two types of vCLVD have been observed⁴⁵, characterised by a vertical pressure (P) or a vertical tension (T) axis^{45,86}. These two mechanisms can result from different configurations, depending on the ring fault geometry and the movement of the inner crustal block: the first case (vertical P) can either be explained by the uplift of the inner block along an outward dipping ring fault, or by its subsidence along an inward dipping fault, while the opposite applies for the second case. The mechanism associated with the slip of a ring segment includes double couple and non double couple components⁸⁵ and the resulting moment tensor can be potentially used to estimate the arc angle and orientation of the ring fault segment⁸⁶. There are several examples of Mw > 5 ring fault earthquakes⁴⁵, often characterised by slow processes or long rupture durations⁴⁶, including some sites where a reversed motion has been observed at the time of uplift and caldera collapse, such as at Bardarbunga volcano, Iceland^{87–89}.

Dike-parallel joints

One of the models proposed to explain focal mechanism reversal at neighbouring locations in volcanic environments and thus, potentially, anti-correlated waveforms, suggests that these earthquakes may occur along neighbouring, subparallel faults at the tip of a propagating dike or near dike constrictions³⁸. The model, sketched in Fig. 2e, hypothesises the activation of sub-parallel structures at the dike tip sides. While this model may be questionable when a magma dike propagates within an undisturbed crustal volume, where fractures at the dike tip are expected to occur along 45° oriented planes^{70,74}, the model could still hold in the case of pre-existing zone of weaknesses or en-echelon structures in strongly heterogeneous stress field, for example due to previous magmatic intrusion episodes, or through the asymmetric failure of solidified magma plugs along magma conduits or channels³⁸.

Overshooting

In tectonic environments, a mechanism able to produce a stress reversal and the activation of earthquakes with similar locations and heterogeneous focal mechanisms, can be given by the occurrence of a large earthquake. Indeed, very diverse focal mechanisms, including cases of focal mechanism reversals, have been observed after large earthquakes, such as the 2011 Tohoku-Oki⁴⁷, Japan, and 2014 Iquique⁴⁸, Chile, earthquakes. In all these reported cases, event pairs with almost reversed focal mechanisms have been located close to each other, either on the same fault or subduction interface, or pre-existing adjacent faults with slightly deviating orientations^{47,48}. In both cases, anti-repeating earthquakes can be explained (Fig. 2f) by a transient reversal of the stress condition, resulting from a complete stress drop and dynamic overshoot⁴⁷.

Fluid injection

There are multiple reports on induced microseismic events with opposite failure mechanisms from hydraulic fracturing operations in shale gas reservoirs^{52–54}. The authors report on dip-slip mechanisms with a steep dipping and an almost horizontal nodal plane, which show both normal or reverse fault motions. The observation of these reversed events has been attributed to the presence of hydraulic fractures that alter the local stress field or directly impose additional strain⁵³, causing an opposite sense of slip. The following models require the presence of particularly oriented weak planes and pre-existing faults. In one model⁵⁴, the opposite slip occurs at shale bedding planes (Fig. 2g). While the opening of the vertical hydraulic fracture itself is considered as an aseismic process, it may produce shear loading on the weaker bedding planes. As a consequence, events with opposite slip directions can be induced in two configurations (Fig. 2g): (a) on two sites of a single bedding plane separated by the hydraulic fracture or (b) on two

closely-located bedding planes at the top and the bottom of the vertical hydraulic fracture, as observed via a clear depth separation for a stage at the Barnett shale^{53,54}. These induced shear events are limited to the vicinity of the hydraulic fracture because no regional shear stress is acting on the bedding planes in this setting⁵⁴. In the case of a horizontally-laying hydraulic fracture opening parallel to the bedding plane, the model must be rotated by 90 degrees (Fig. 2h). Consequently, the additional stress at the fracture tips could produce or reactivate a micro-graben structure with an opposite slip direction on possibly close-by, nearly vertical, pre-existing natural fractures⁵².

Discussion

In this work, we reported several observations of earthquake pairs with anti-correlated waveforms, which we attribute to true or quasi anti-repeating earthquakes. Our observations are quite heterogeneous. First, they sample very different seismogenic environments, with seismicity either controlled by tectonic, volcanic or anthropogenic processes. Further, the presented case studies concern a broad range of magnitudes, inter-event times, and observational setups. A general conclusion is that not only do (true and/or quasi) anti-repeating earthquakes exist, but they can even be found in very different seismogenic contexts.

Many of the observations shown in Fig. 1 can be directly explained by the proposed source models, controlled by spatiotemporal stress perturbation introduced by fluid transfer. For example, parallel normal and thrust faulting at the North Mid Atlantic Ridge (Fig. 1a) have been explained in response to a dike intrusion (Fig. 2a, b), with normal faulting occurring shallow above the vertical dike and thrust faulting occurring at its both sides⁵⁶. In the case of the Mayotte anti-repeaters (Fig. 1c), the seismogenic process is likely related to the overall depletion of a deep magma reservoir²⁷; it has been suggested that pressure fluctuations within the depleting reservoir could promote short-term stress transients in the overburden, accommodated by upward and downward movement of trapdoor fault(s) (Fig. 2c) with short inter-event times²⁷. The observation at the Äspö Rock Laboratory (Fig. 1d) is most likely attributed to a local stress rotation induced by the growth of a hydraulic fracture, a small scale equivalent to a dike intrusion (Fig. 2a, b). The observation of heterogeneous focal mechanisms within the compact Bucaramanga nest, including anti-repeaters (Fig. 1b), remains poorly understood²⁴.

For earthquake repeaters, highly correlating waveforms imply that their inter-source distance is smaller than a quarter of a wavelength¹. The same threshold applies for anti-repeaters: in our cases, such a spatial threshold reaches from tens of centimetres to tens of kilometres (Table 1). High anti-correlation values and small inter-event distances below or close to the respective quarter-wavelength criterion in all cases (Table 1) suggest anti-repeaters. However, to resolve if the earthquake rupture patches are overlapping, and not just close, frequencies should be chosen high enough²². Additional information from accurate location might resolve inter-event distances, helping discriminating true and quasi anti-repeaters^{1–3}. However, location uncertainties may often be larger than the spatial separation of event hypocenters, hindering a robust identification of true anti-repeaters. One of those cases showing a large spatial separation between epicenters is the example from the Mid-Atlantic ridge, which is in fact a case of quasi anti-repeater associated with the reverse motion of neighbouring faults⁵⁶. For the Mayotte case, where the inter-event distance exceeds 600 m, the rupture patches may be very close but likely not overlapping. At the Bucaramanga nest, it has been reported that an overlap of the rupture areas cannot be resolved²⁴. Similar limitations apply to the Äspö Hard Rock Laboratory, where the inter-event distance is smaller than the location uncertainty⁶⁶. The physical models compiled in this study also concern both true anti-repeaters and quasi-anti-repeaters. True anti-repeater could occur, for example, along the same ring fault, as a consequence of inflation and deflection periods of an underground magma reservoir (Fig. 2d). Conversely, other models, such as the triggering of normal vs thrust faulting above or on the side of a dike, only explain quasi anti-repeaters. We like to point out that the separation of true and quasi anti-repeaters is less critical at this point compared to repeating

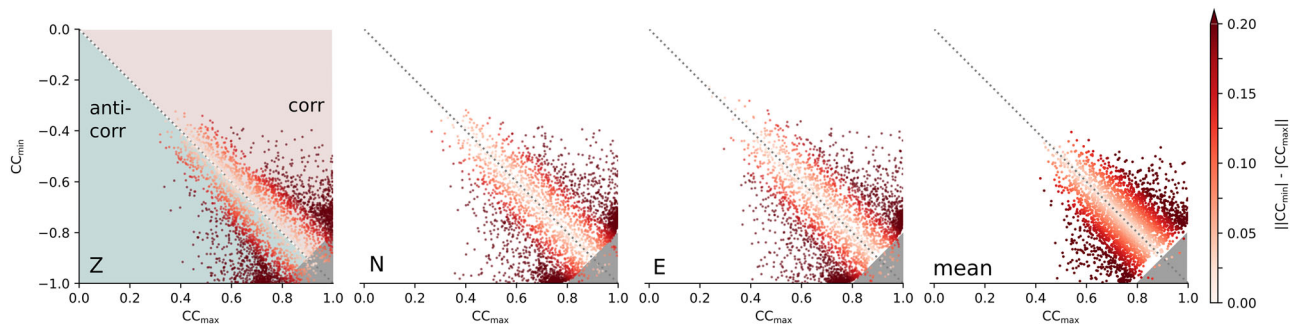


Fig. 3 | Synthetic tests. A comparison of minimum and maximum CC for synthetic waveforms of 3000 random double couple (DC) sources randomly co-located at a distance of 30 km around a central receiver. CC_{\min} is plotted over CC_{\max} for three components and for their mean, colour-coded according to the difference of the

absolute values of CC_{\min} and CC_{\max} . The lower triangle shows events which show higher anti-correlations (larger absolute CC_{\min}), while higher correlation (larger absolute CC_{\max}) are in the upper triangle. The critical region for the identification (anti-)repeaters is marked by a grey triangle.

events, e.g., used to quantify fault creep or predominantly aseismic processes: in both cases, stress transients cause a remarkable change of local stress conditions.

Since the local stress conditions control the fault motion during an earthquake, a motion reversal along the same fault segment would require a substantial temporal stress change. Should the two reversed earthquakes occur along neighbouring structures, rather than a single one, the proposed models explain this by the presence of a strong stress heterogeneity in the focal region. Therefore, studying true and quasi anti-repeaters is important to detect spatial and/or temporal anomalies of the stress condition. In the case of tectonically active regions, the stress anomaly can be due to the occurrence of a large earthquake^{47,48} (Fig. 2f). However, in most reported cases, including those occurring in volcanic environments or associated with injection-induced seismicity, the stress transient is rather attributed to fluid migration processes. In these cases, the observation of anti-repeaters provides indirect evidence for the presence of fluid and its migration. This may also apply to the case of intermediate and deep seismicity, which are often attributed to dehydration processes, e.g., for the Bucaramanga nest.

Previous works on repeating earthquakes have often neglected the presence of anti-correlating signals. The minimum and the maximum of the cross-correlation of two waveforms depends on the frequency content and the chosen time window: higher frequencies, sampling smaller local structures, and longer time windows containing more noise reduce both values. Additionally, the definition of a high cross-correlation varies across different studies^{2,22}, as does the threshold for which waveforms are considered to be similar⁹⁰. With a simple synthetic test (Fig. 3), we show that even relatively high maximum cross-correlation values (such as 0.8) can be misleading when omitting the negative part of the cross-correlation function or using the absolute value. Of course, the validity of not considering the negative part depends on the purpose of the study. Still, it is a loss of information that might have hindered broader attention to anti-correlated events/anti-repeaters in the past. For the test, we calculated synthetic three-component waveforms (up to 4 Hz) for two co-located random double-couple mechanisms based on a regional velocity model for Mayotte²⁷. The synthetics are calculated using the pyrocko toolbox and a precalculated Green's function database⁹¹ obtained via the orthonormal propagator algorithm QSEIS⁹². We choose a geometrical setup that mimics the observational condition of the Mayotte case: the epicentral distance of the receiver is fixed at 30 km, while the event depth is randomly chosen from a uniform distribution between 1 and 50 km, as is the event azimuth relative to the receiver. Maximum and minimum cross-correlation values are plotted for each spatial component (Z, vertical, N, North, E, East) and their mean value in Fig. 3. Since we consider the full cross-correlation function, the minimum cross-correlation value (CC_{\min}) is the amplitude of the largest negative lobe of the cross-correlation function, not the lowest correlation. The colour scale is chosen so that dark red points highlight waveforms where the difference between the absolute values of CC_{\min} and CC_{\max} is larger. The upper

triangle corresponds to waveform correlation, where the absolute value of CC_{\max} is larger than for CC_{\min} , while the lower triangle corresponds to waveform anti-correlation. The plot is illustrative of the potential pitfalls when considering only positive cross-correlation values: using only single components, CC_{\max} can be as high as 0.85/0.9, which could support the identification of a repeater, but still CC_{\min} is close to -1 , showing that, in fact, this is rather supporting an anti-repeater (see also Suppl. Fig. 9). Combining the three components by calculating their respective means helps isolate (anti-)repeaters more clearly. Including more stations in the (anti-)repeaters analysis can further increase the reliability of the results. When using three components, single anti-correlated event pairs can still appear highly correlated (within the grey triangle in Fig. 3). After all, we show that an (almost) perfect anti-repeater could be lost in favour of a less-well constrained repeater or not recognized at all if omitting the negative part of the cross-correlation. An example of a highly anticorrelated pair of events from the synthetic test that would be missed and labelled as a pair of similar events when only considering the positive part of the CC function is provided in the supplement (Suppl. Fig. 9).

While we focus on single earthquake pairs in this study and review them manually, a comprehensive search for anti-correlated events would require additional quality tests for an unambiguous identification of (anti-)repeaters. Signals with limited, narrow bandwidth originating from the source or caused by local site effects can lead to cycle skipping when dominant subsequent peaks get misaligned⁹³. An extreme case would be a monotonic signal that can be shifted arbitrarily. Cycle skipping biasing the cross-correlation coefficient can be accounted for by testing different time windows and only accepting CCs that show consistent results, e.g., satisfying a maximum time shift depending on the event duration, the frequency content, and the data sampling, over multiple window lengths^{90–93}. A SNR-based threshold to exclude waveforms prone to cycle skipping before calculating the cross-correlation and a time-independent criterion for the comparison of the maximum and the second largest peak (sidelobe maximum, CC_{slm} , corresponding to the largest positive value of the cross-correlation function in the case of anti-repeaters) of the cross-correlation function, $CC_{\text{slm}} < CC - (0.5 - 0.5 CC)$, have been suggested⁹⁴. All example cases in this study pass the time-independent cycle skipping criterion. In our synthetic test (Fig. 3), cycle skipping becomes problematic for those event pairs marked by light red points.

Small differences between the absolute values of CC_{\min} and CC_{\max} , which we refer to here as differential cross-correlation coefficient, might hinder an unambiguous identification of (anti-)repeaters. In the example shown in this study, the differential cross-correlation ranges between 0.08 and 0.35 (Table 1). A small differential cross-correlation coefficient can point to spurious correlations caused by a monotonic signal or a small number of data samples, thus a short time window. This implies that a threshold needed to achieve a robust identification of (anti-)repeaters depends on the complexity and the length of the cross-correlated seismograms. In this study, all cross-correlations of the example cases were

calculated using full-waveforms with approximately 1000 samples which ensures a robust identification of (quasi) anti-repeaters. The synthetic test shows that identifying (anti-)repeaters is possible with only one three-component station. However, single-station analyses might suffer from low signal-to-noise ratios on any component depending on the radiation pattern of the studied earthquake mechanism. If the data are available, repeaters and anti-repeaters should be identified using multiple seismic records from stations around the epicentres since increased azimuthal coverage provides more robust results⁹⁵.

Conclusions

In this work we proved the widespread existence of earthquake pairs with highly anti-correlated waveforms in a multitude of seismological settings. Although negative waveform cross-correlations have been rarely considered in seismological analysis, we illustrate that several such observations are already available. The reported case studies sample a wide variety of environments where events with anti-correlated waveforms can be observed, including volcanic, tectonic and induced seismicity, as well as shallow and intermediate depth seismicity. This implies that anti-repeaters may occur in almost any seismogenic context. The limited amount of references reporting this type of observations is possibly only due to the fact that scientists have not yet carefully considered anti-correlated waveforms. The set of reported case studies concerns a broad range of magnitudes, spanning from micro-seismicity associated to fluid injection operations up to earthquakes of magnitudes Mw 6.0, e.g., at the Mid Atlantic ridge. Differential times among event pairs are also very variable. In some cases, as, for example, at Mayotte, they occur with short delays in the order of seconds to minutes. In other cases, such as at Bucaramanga, the delay is in the order of years.

Besides reporting on different observations of events with anti-correlated waveforms, we reviewed previously proposed models. Both observations and models illustrate the presence of two different scenarios. On one side, there are true anti-repeaters, which affect the same fault or fault segment with a reverse motion, implying a process reversal; these can occur, for example, in the case of trapdoor or ring-faulting in response to pressurisation or depressurization of magmatic reservoirs and conduits. In many cases, however, we observe so-called quasi anti-repeaters, which have a reversed focal mechanism but occur on neighbouring structures. These earthquakes can be modelled, for example by the reversed activation of parallel faults in response to magma dike intrusions.

In the lack of dedicated, local monitoring, location uncertainties may challenge the discrimination between true and quasi anti-repeaters. However, both of them denote the presence of strong spatial and/or temporal stress perturbations, for example in response to a magmatic intrusion or to a large earthquake. Thus, they can directly be used to detect stress perturbations in space and time. In many cases, especially in the frame of volcanic and induced seismogenic processes, they are directly controlled by fluid transfer. In these environments, the identification of anti-repeater provides valuable information to track underground fluids and their movements.

Supplementary Material

The supplementary material includes 9 Suppl. Figs. which complement the main text.

Data availability

Seismic data used in this study pertains to the following networks: RA (RESIF-RAP Accelerometric Permanent Network 1995)⁹⁶, CM (Red Sismológica Nacional de Colombia)⁹⁷, G (GEOSCOPE, French Global Network of Seismological Broadband Stations)⁵⁷. These data are open and available at IRIS (Incorporated Research Institutions for Seismology), GEOFON (GEO-ForschungsNetz), ORFEUS EIDA (Observatories and Research Facilities for European Seismology - European Integrated Data Archive) and/or Résif - Réseau sismologique et géodésique français⁹⁶ web services. Waveform data for the anti-repeaters recorded during the injection experiments at the Äspö Hard Rock Laboratory are available via the data publication⁹⁸.

Code availability

All software used in this work is open source. The codes used to generate each figure and result are available through the contact information from the original publications. Requests for further materials should be directed to S.C. (simone.cesca@gfz-potsdam.de).

Received: 12 September 2023; Accepted: 27 February 2024;

Published online: 27 March 2024

References

1. Waldhauser, F. & Schaff, D. P. A comprehensive search for repeating earthquakes in northern California: Implications for fault creep, slip rates, slip partitioning, and transient stress. *J. Geophys. Res.: Solid Earth* **126**, e2021JB022495 (2021).
2. Gao, D., Kao, H. & Wang, B. Misconception of waveform similarity in the identification of repeating earthquakes. *Geophys. Res. Lett.* **48**, e2021GL092815 (2021).
3. Gao, D., Kao, H. & Liu, J. Identification of repeating earthquakes: controversy and rectification. *Seismol. Res. Lett.* **94**, 2655–2665 (2023).
4. Geller, R. J. & Mueller, C. S. Four similar earthquakes in central California. *Geophys. Res. Lett.* **7**, 821–824 (1980).
5. Vidale, J. E., Ellsworth, W. L., Cole, A. & Marone, C. Variations in rupture process with recurrence interval in a repeated small earthquake. *Nature* **368**, 624–626 (1994).
6. Nadeau, R., Antolik, M., Johnson, P. A., Foxall, W. & McEvilly, T. V. Seismological studies at Parkfield III: microearthquake clusters in the study of fault-zone dynamics. *Bull. Seismol. Soc. Am.* **31**, 271 (1994).
7. Ellsworth, W. L. Characteristic earthquakes and long-term earthquake forecasts: Implications of central California seismicity. In *Urban Disaster Mitigation: The Role of Engineering and Technology* (eds Cheng, F. Y. & Sheu, M.-S.) 1–14 (Pergamon, 1995).
8. Bakun, W. H., King, G. C. & Cockerham, R. S. Seismic slip, aseismic slip, and the mechanics of repeating earthquakes on the Calaveras Fault, California. In *Earthquake Source Mechanics*, Vol. 37 (eds Das, S., Boatwright, J. & Scholz, C. H.) 195–207, (AGU, Washington, D. C., 1986).
9. Schmittbuhl, J., Karabulut, H., Lengliné, O. & Bouchon, M. Long-lasting seismic repeaters in the Central Basin of the Main Marmara fault. *Geophys. Res. Lett.* **43**, 9527–9534 (2016).
10. Mesimeri, M. & Karakostas, V. Repeating earthquakes in western Corinth Gulf (Greece): Implications for aseismic slip near locked faults. *Geophys. J. Int.* **215**, 659–676 (2018).
11. Igarashi, T., Matsuzawa, T. & Hasegawa, A. Repeating earthquakes and interplate aseismic slip in the northeastern Japan subduction zone. *J. Geophys. Res.: Solid Earth* **108**, B5 (2003).
12. Uchida, N. & Matsuzawa, T. Coupling coefficient, hierarchical structure, and earthquake cycle for the source area of the 2011 off the Pacific coast of Tohoku earthquake inferred from small repeating earthquake data. *Earth Planets Sp.* **63**, 675–679 (2011).
13. Nadeau, R. M. & Johnson, L. R. Seismological studies at Parkfield VI: moment release rates and estimates of source parameters for small repeating earthquakes. *Bull. seism. Soc. Am.* **88**, 790–814 (1998).
14. Nadeau, R. M. & McEvilly, T. V. Fault slip rates at depth from recurrence intervals of repeating microearthquakes. *Science* **285**, 718–721 (1999).
15. Bouchon, M. et al. Extended nucleation of the 1999 Mw 7.6 Izmit earthquake. *Science* **331**, 877–880 (2011).
16. Ellsworth, W. L. & Bulut, F. Nucleation of the 1999 Izmit earthquake by a triggered cascade of foreshocks. *Nat. Geosci.* **11**, 531–535 (2018).
17. Poupinet, G., Ellsworth, W. L. & Frechet, J. Monitoring velocity variations in crust using earthquake doublets: an application to the Calaveras fault, California. *J. Geophys. Res.* **89**, 5719–5731 (1984).
18. Harris, D. B. A waveform correlation method for identifying quarry explosions. *Bull. Seismol. Soc. Am.* **81**, 2395–2418 (1991).

19. Rubin, A. M., Gillard, D. & Got, J. L. A reinterpretation of seismicity associated with the January 1983 dike intrusion at Kilauea Volcano, Hawaii. *J. Geophys. Res.: Solid Earth* **103**, 10003–10015 (1998).
20. Lees, J. M. Multiplet analysis at Coso geothermal. *Bull. Seismol. Soc. Am.* **88**, 1127–1143 (1998).
21. Moriya, H. Multiplet-clustering analysis reveals structural details within the seismic cloud at the Soutz geothermal field, France. *Bull. Seismol. Soc. Am.* **93**, 1606–1620 (2003).
22. Uchida, N. & Bürgmann, R. Repeating earthquakes. *Annu. Rev. Earth Planet. Sci.* **47**, 305–332 (2019).
23. Barrett, S. A., Prieto, G. & Beroza, G. C. Detection of repeating and “anti-repeating” earthquakes in the Bucaramanga Nest. *AGU Fall Meeting Abstracts* **2011**, T13A–T12350 (2011).
24. Prieto, G. A., Beroza, G. C., Barrett, S. A., López, G. A. & Florez, M. Earthquake nests as natural laboratories for the study of intermediate-depth earthquake mechanics. *Tectonophysics* **570–571**, 42–56 (2012).
25. Cassidy, J. F. et al. The 2007 Nazko, British Columbia, earthquake sequence: injection of magma deep in the crust beneath the Anahim Volcanic Belt. *Bull. Seismol. Soc. Am.* **101**, 1732–1741 (2011).
26. Hotovec-Elis, A. J. et al. Deep fluid pathways beneath Mammoth Mountain, California, illuminated by migrating earthquake swarms. *Sci. Adv.* **4**, eaat5258 (2018).
27. Cesca, S. et al. Drainage of a deep magma reservoir near Mayotte inferred from seismicity and deformation. *Nat. Geosci.* **13**, 87–93 (2020).
28. Lemoine, A. et al. The 2018–2019 seismo-volcanic crisis east of Mayotte, Comoros islands: seismicity and ground deformation markers of an exceptional submarine eruption. *Geophys. J. Int.* **223**, 22–44 (2020).
29. Feuillet, N. et al. Birth of a large volcanic edifice offshore Mayotte via lithosphere-scale dyke intrusion. *Nat. Geosci.* **14**, 787–795 (2021).
30. Shelly, D. R., Hardebeck, J. L., Ellsworth, W. L. & Hill, D. P. A new strategy for earthquake focal mechanisms using waveform-correlation-derived relative polarities and cluster analysis: Application to the 2014 Long Valley Caldera earthquake swarm: a new strategy for focal mechanisms. *J. Geophys. Res. Solid Earth* **121**, 8622–8641 (2016).
31. Ide, S., Shelly, D. R. & Beroza, C. B. Mechanism of deep low frequency earthquakes: Further evidence that deep non-volcanic tremor is generated by shear slip on the plate interface. *Geophys. Res. Lett.* **34**, L03308 (2007).
32. Bonaccorso, A., Ferrucci, F., Patané, D. & Villari, L. Fast deformation processes and eruptive activity at Mount Etna (Italy). *J. Geophys. Res.: Solid Earth* **101**, 17467–17480 (1996).
33. Roman, D. C. Temporal and spatial variation of local stress fields before and after the 1992 eruptions of Crater Peak vent, Mount Spurr volcano, Alaska. *Bull. Seismol. Soc. Am.* **94**, 2366–2379 (2004).
34. Smith, K. D. et al. Evidence for deep magma injection beneath Lake Tahoe, Nevada-California. *Science* **305**, 1277–1280 (2004).
35. Roman, D. C. & Cashman, K. V. The origin of volcano-tectonic earthquake swarms. *Geology* **34**, 457–460 (2006).
36. Roman, D. C., Neuberg, J. & Luckett, R. R. Assessing the likelihood of volcanic eruption through analysis of volcanotectonic earthquake fault-plane solutions. *Earth Planet. Sci. Lett.* **248**, 244–252 (2006).
37. von Seggern, D. H., Smith, K. D. & Preston, L. A. Seismic spatial-temporal character and effects of a deep (25–30 km) magma intrusion below North Lake Tahoe, California–Nevada. *Bull. Seismol. Soc. Am.* **98**, 1508–1526 (2008).
38. White, R. S. et al. Dynamics of dyke intrusion in the mid-crust of Iceland. *Earth Planet. Sci. Lett.* **304**, 300–312 (2011).
39. Shelly, D. R. & Hill, D. P. Migrating swarms of brittle-failure earthquakes in the lower crust beneath Mammoth Mountain, California. *Geophys. Res. Lett.* **38**, n/a (2011).
40. Smith, K. D., Kent, G. M., von Seggern, D. P., Driscoll, N. W. & Eisses, A. Evidence for Moho-lower crustal transition depth diking and rifting of the Sierra Nevada microplate. *Geophys. Res. Lett.* **43**, 10–738 (2016).
41. Roman, D. C., Soldati, A., Dingwell, D. B., Houghton, B. F. & Shiro, B. R. Earthquakes indicated magma viscosity during Kilauea’s 2018 eruption. *Nature* **592**, 237–241 (2021).
42. Del Fresno, C. et al. Magmatic plumbing and dynamic evolution of the 2021 La Palma eruption. *Nat. Commun.* **14**, 358 (2023).
43. Donner, S. et al. The January 2022 Hunga Volcano explosive eruption from the multitechnological perspective of CTBT monitoring. *Geophys. J. Int.* **235**, 48–73 (2023).
44. Rutledge, J. T. Faulting induced by forced fluid injection and fluid flow forced by faulting: an interpretation of hydraulic-fracture microseismicity, Carthage Cotton Valley gas field, Texas. *Bull. Seismol. Soc. Am.* **94**, 1817–1830 (2004).
45. Shuler, A., Nettles, M. & Ekström, G. Global observation of vertical-CLVD earthquakes at active volcanoes. *J. Geophys. Res. Solid Earth* **118**, 138–164 (2013).
46. Shuler, A., Ekström, G. & Nettles, M. Physical mechanisms for vertical-CLVD earthquakes at active volcanoes. *J. Geophys. Res. Solid Earth* **118**, 1569–1586 (2013).
47. Ide, S., Baltay, A. & Beroza, G. C. Shallow dynamic overshoot and energetic deep rupture in the 2011 M w 9.0 Tohoku-Oki earthquake. *Science* **332**, 1426–1429 (2011).
48. Cesca, S. et al. The M w 8.1 2014 Iquique, Chile, seismic sequence: a tale of foreshocks and aftershocks. *Geophys. J. Int.* **204**, 1766–1780 (2016).
49. Skoumal, R. J., Brudzinski, M. R. & Currie, B. S. An efficient repeating signal detector to investigate earthquake swarms. *J. Geophys. Res. Solid Earth* **121**, 5880–5897 (2016).
50. Schultz, R. et al. Hydraulic fracturing-induced seismicity. *Rev. Geophys.* **58**, e2019RG000695 (2020).
51. Majer, E. L. et al. Induced seismicity associated with Enhanced Geothermal Systems. *Geothermics* **36**, 185–222 (2007).
52. Eisner, L., Williams-Stroud, S., Hill, A., Duncan, P. & Thornton, M. Beyond the dots in the box: microseismicity-constrained fracture models for reservoir simulation. *The Leading Edge* **29**, 326–333 (2010).
53. Rutledge, J., Yu, X. & Leaney, S. Microseismic shearing driven by hydraulic-fracture opening: an interpretation of source-mechanism trends. *The Leading Edge* **34**, 926–934 (2015).
54. Staněk, F. & Eisner, L. Seismicity induced by hydraulic fracturing in shales: a bedding plane slip model: a bedding plane slip model. *J. Geophys. Res. Solid Earth* **122**, 7912–7926 (2017).
55. Frohlich, C. & Nakamura, Y. The physical mechanisms of deep moonquakes and intermediate-depth earthquakes: How similar and how different? *Phys. Earth Planetary Interiors* **173**, 365–374 (2009).
56. Cesca, S., Metz, M., Büyükakpınar, P. & Dahm, T. The energetic 2022 seismic unrest related to magma intrusion at the North Mid-Atlantic Ridge. *Geophys. Res. Lett.* **50**, e2023GL102782 (2023).
57. Institut de physique du globe de Paris (IPGP), & École et Observatoire des Sciences de la Terre de Strasbourg (EOST). (1982). *GEOSCOPE, French Global Network of broad band seismic stations*. Institut de physique du globe de Paris (IPGP), Université de Paris. <https://doi.org/10.18715/GEOSCOPE.G>.
58. Zarifi, Z. & Havskov, J. Characteristics of dense nests of deep and intermediate-depth seismicity. *Adv. Geophys.* **46**, 238–278 (2003).
59. Prieto, G. A. et al. Seismic evidence for thermal runaway during intermediate-depth earthquake rupture. *Geophys. Res. Lett.* **40**, 6064–6068 (2013).
60. Frohlich, C. *Deep earthquakes* (Cambridge University Press, 2006).

61. Schneider, J. F., Pennington, W. D. & Meyer, R. P. Microseismicity and focal mechanisms of the intermediate-depth Bucaramanga Nest, Colombia. *J. Geophys. Res.: Solid Earth* **92**, 13913–13926 (1987).
62. Blaser, L., Kruger, F., Ohrnberger, M. & Scherbaum, F. Scaling relations of earthquake source parameter estimates with special focus on subduction environment. *Bull. Seismol. Soc. Am.* **100**, 2914–2926 (2010).
63. Cesca, S. et al. (2019) Seismic catalogues of the 2018–2019 volcano-seismic crisis offshore Mayotte, Comoro Islands. V. 1.0 (October 2019). GFZ Data Services. <https://doi.org/10.5880/GFZ.2.1.2019.004>.
64. Mercury, N. et al. Onset of a submarine eruption east of Mayotte, Comoros archipelago: the first ten months seismicity of the seismo-volcanic sequence (2018–2019). *Comptes Rendus. Géosci.* **354**, 105–136 (2022).
65. Zang, A. et al. Hydraulic Fracture Monitoring in Hard Rock at 410 m Depth with an Advanced Fluid-Injection Protocol and Extensive Sensor Array. *Geophys. J. Int.* **208**, 790–813 (2017).
66. Niemz, P. et al. Full-waveform-based characterization of acoustic emission activity in a mine-scale experiment: a comparison of conventional and advanced hydraulic fracturing schemes. *Geophys. J. Int.* **222**, 189–206 (2020).
67. Niemz, P. et al. Insights into hydraulic fracture growth gained from a joint analysis of seismometer-derived tilt signals and acoustic emissions. *J. Geophys. Res. Solid Earth* **126**, e2021JB023057 (2021).
68. Kwiatek, G. et al. Insights into complex subdecimeter fracturing processes occurring during a water injection experiment at depth in Äspö Hard Rock Laboratory, Sweden. *J. Geophys. Res. Solid Earth* **123**, 6616–6635 (2018).
69. Zang, A. et al. Relaxation damage control via fatigue-hydraulic fracturing in granitic rock as inferred from laboratory-, mine-, and field-scale experiments. *Scientific Reports* **11**, 6780 (2021).
70. Hill, D. P. A model for earthquake swarms. *J. Geophys. Res.* **82**, 1347–1352 (1977).
71. Rubin, A. M. & Pollard, D. D. Dike-induced faulting in rift zones of Iceland and Afar. *Geology* **16**, 413–417 (1988).
72. Ukawa, M. & Tsukahara, H. Earthquake swarms and dike intrusions off the east coast of Izu Peninsula, central Japan. *Tectonophysics* **253**, 285–303 (1996).
73. Roman, D. C. Numerical models of volcanotectonic earthquake triggering on non-ideally oriented faults. *Geophys. Res. Lett.* **32**, L02304 (2005).
74. Passarelli, L., Rivalta, E., Cesca, S. & Aoki, Y. Stress changes, focal mechanisms, and earthquake scaling laws for the 2000 dike at Miyakejima (Japan). *J. Geophys. Res. Solid Earth* **120**, 4130–4145 (2015).
75. Rubin, A. M. Propagation of magma-filled cracks. *Annual Rev. Earth Planetary Sci.* **23**, 287–336 (1995).
76. Fukuyama, E., Kubo, A., Kawai, H. & Nonomura, K. Seismic remote monitoring of stress field. *Earth Planets Space* **53**, 1021–1026 (2001).
77. Umakoshi, K., Shimizu, H. & Matsuwo, N. Volcano-tectonic seismicity at Unzen Volcano, Japan, 1985–1999. *J. Volcanol. Geotherm. Res.* **112**, 117–131 (2001).
78. Legrand, D. et al. Stress tensor analysis of the 1998–1999 tectonic swarm of northern Quito related to the volcanic swarm of Guagua Pichincha volcano, Ecuador. *Tectonophysics* **344**, 15–36 (2002).
79. Roman, D. C., Neuberg, J., Luckett, R. R. & White, R. A. Changes in the orientation of local stresses prior to and during magmatic activity at the Soufrière Hills Volcano, Montserrat. *Eos (Transactions, American Geophysical Union)* **v. 86**, V21C–V20622 (2005).
80. Amelung, F., Jónsson, S., Zebker, H. & Segall, P. Widespread uplift and ‘trapdoor’ faulting on Galapagos volcanoes observed with radar interferometry. *Nature* **407**, 993–996 (2000).
81. Fialko, Y. On origin of near-axis volcanism and faulting at fast spreading mid-ocean ridges. *Earth Planetary Sci. Lett.* **190**, 31–39 (2001).
82. Jónsson, S., Zebker, H. & Amelung, F. On trapdoor faulting at Sierra Negra volcano, Galápagos. *J. Volcanol. Geotherm. Res.* **144**, 59–71 (2005).
83. Sandanbata, O. et al. Sub-decadal volcanic tsunamis due to submarine trapdoor faulting at Sumisu Caldera in the Izu–Bonin Arc. *J. Geophys. Res. Solid Earth* **127**, e2022JB024213 (2022).
84. Sandanbata, O., Watada, S., Satake, K., Kanamori, H. & Rivera, L. Two volcanic tsunami events caused by trapdoor faulting at a submerged caldera near Curtis and Cheeseman Islands in the Kermadec Arc. *Geophys. Res. Lett.* **50**, e2022GL101086 (2023).
85. Cesca, S. & Heimann, S. Challenges in regional moment tensor resolution and interpretation. In *Moment Tensor Solutions: A Useful Tool for Seismotectonics* (ed. D’Amico, S.) 163–181 (2018). https://doi.org/10.1007/978-3-319-77359-9_7.
86. Sandanbata, O. et al. Moment tensors of ring-faulting at active volcanoes: Insights into vertical-CLVD earthquakes at the Sierra Negra caldera, Galápagos Islands. *J. Geophys. Res. Solid Earth* **126**, e2021JB021693 (2021).
87. Nettles, M. & Ekström, G. Faulting mechanism of anomalous earthquakes near Bárðarbunga Volcano, Iceland. *J. Geophys. Res. Solid Earth* **103**, 17973–17983 (1998).
88. Gudmundsson, M. T. et al. Gradual caldera collapse at Bárðarbunga volcano, Iceland, regulated by lateral magma outflow. *Science* **353**, aaf8988 (2016).
89. Glastonbury-Southern, E., Winder, T., White, R. S. & Brandsdóttir, B. Ring Fault Slip Reversal at Bárðarbunga Volcano, Iceland: seismicity during caldera collapse and re-inflation 2014–2018. *Geophys. Res. Lett.* **49**, e2021GL097613 (2022).
90. Schaff, D. P. Waveform cross-correlation-based differential travel-time measurements at the Northern California seismic network. *Bull. Seismol. Soc. Am.* **95**, 2446–2461 (2005).
91. Heimann, S. et al. A Python framework for efficient use of pre-computed Green’s functions in seismological and other physical forward and inverse source problems. *Solid Earth* **10**, 1921–1935 (2019).
92. Wang, R. A simple orthonormalization method for stable and efficient computation of Green’s functions. *Bull. Seismol. Soc. Am.* **89**, 733–741 (1999).
93. Akuhara, T. & Mochizuki, K. Application of cluster analysis based on waveform cross-correlation coefficients to data recorded by ocean-bottom seismometers: results from off the Kii Peninsula. *Earth Planets Sp.* **66**, 80 (2014).
94. Diehl, T., Kraft, T., Kissling, E. & Wiemer, S. The induced earthquake sequence related to the St. Gallen deep geothermal project (Switzerland): Fault reactivation and fluid interactions imaged by microseismicity. *J. Geophys. Res.: Solid Earth* **122**, 7272–7290 (2017).
95. Petersen, G. M., Niemz, P., Cesca, S., Mouslopoulou, V. & Bocchini, G. M. Clusty, the waveform-based network similarity clustering toolbox: Concept and application to image complex faulting offshore Zakynthos (Greece). *Geophys. J. Int.* **224**, 2044–2059 (2020).
96. RESIF-RAP Accelerometric Permanent Network (RESIF, RESIF-RAP French Accelerometric Network, 1995); <https://doi.org/10.15778/RESIF.RA>.
97. Servicio Geológico Colombiano (1993). *Red Sismológica Nacional de Colombia* [Data set]. International Federation of Digital Seismograph Networks. <https://doi.org/10.7914/SN/CM>.
98. Zang, A. et al. Comprehensive data set of in-situ hydraulic stimulation experiments for geothermal purposes at the Äspö Hard Rock Laboratory (Sweden). *Earth Syst. Sci. Data Discuss.* **16**, 295–310 (2024).

Acknowledgements

We are thankful to all institutes providing seismic data used in this study. We are thankful to the Editors Dr. J. Aslin and Prof. Dr. J. Caplan-Auerbach, two anonymous reviewers, as well as, Prof. Dr. D. Stich for their careful reading and valuable suggestions. P.N. received funding from the European Union RFCS project PostMinQuake grant 899192.

Author contributions

S.C. coordinated this project, conceived the manuscript, and analysed seismological data. P.N. performed the analysis of Åspö data. S.C. and P.N. prepared figures; P.N. prepared tables. S.C., P.N., T.D. and S.I. drafted the manuscript. All authors reviewed the manuscript.

Funding

Open Access funding enabled and organized by Projekt DEAL.

Competing interests

The authors declare no competing interests.

Additional information

Supplementary information The online version contains supplementary material available at <https://doi.org/10.1038/s43247-024-01290-1>.

Correspondence and requests for materials should be addressed to Simone Cesca.

Peer review information *Communications Earth & Environment* thanks Jackie Caplan-Auerbach, German Prieto and the other, anonymous, reviewer(s) for their contribution to the peer review of this work. A peer review file is available.

Reprints and permissions information is available at <http://www.nature.com/reprints>

Publisher's note Springer Nature remains neutral with regard to jurisdictional claims in published maps and institutional affiliations.

Open Access This article is licensed under a Creative Commons Attribution 4.0 International License, which permits use, sharing, adaptation, distribution and reproduction in any medium or format, as long as you give appropriate credit to the original author(s) and the source, provide a link to the Creative Commons licence, and indicate if changes were made. The images or other third party material in this article are included in the article's Creative Commons licence, unless indicated otherwise in a credit line to the material. If material is not included in the article's Creative Commons licence and your intended use is not permitted by statutory regulation or exceeds the permitted use, you will need to obtain permission directly from the copyright holder. To view a copy of this licence, visit <http://creativecommons.org/licenses/by/4.0/>.

© The Author(s) 2024